

A Fixed-Point Algorithm for the AC Power Flow Problem

Liangjie Chen and John W. Simpson-Porco

Abstract—This paper presents an algorithm that solves the AC power flow problem for balanced, three-phase transmission systems at steady state. The algorithm extends the “fixed-point power flow” algorithm in the literature to include transmission losses, phase-shifting transformers, and a distributed slack bus model. The algorithm is derived by vectorizing the component-wise AC power flow equations and manipulating them into a novel equivalent fixed-point form. Preliminary theoretical results guaranteeing convergence are reported for the case of a two-bus power system. We validate the algorithm through extensive simulations on test systems of various sizes under different loading levels, and compare its convergence behavior against those of classic power flow algorithms.

I. INTRODUCTION

A fundamental problem which underpins many others in power system operations and control (e.g., optimal power flow, contingency analysis) is that of computing solutions to the power flow equations. These equations describe the flow and balance of power in a synchronous AC power system at steady state [1], and are typically difficult to solve due to the inherently nonlinear relationship between power and voltage. Analytic solutions are rarely available, and solutions are instead computed via numerical methods.

A plethora of heuristics and algorithms for analyzing power flow have been developed [2]–[5]. The most standard approach to accurately solve the power flow problem is to use an iterative algorithm such as Newton-Raphson (NR) [1, Chapter 6]. The NR algorithm in particular is highly sensitive to initialization [6], and heuristic or approximation procedures are sometimes needed to find suitable initial conditions [7], [8]. More generally, when iterative algorithms fail, the failure mechanism can be difficult to determine, in that one cannot distinguish between poor initialization and an infeasible power flow case. Thus, a robust algorithm for the power flow problem with transparent conditions for convergence is highly desirable.

In recent years, there have been many fixed-point or contraction-based studies on the power flow problem and its solvability in various contexts (see, e.g., [9]–[12]). These approaches provide sufficient conditions for the existence (and often, uniqueness) of a suitable power flow solution, and the contraction property naturally leads to a fixed-point iteration for computing that solution, which is guaranteed to converge from any initialization within the contraction region. Among these studies, our focus is power flow in balanced AC transmission systems. A recently developed research direction resulted in novel and particularly robust

fixed-point based algorithms, termed fixed-point power flow (FPPF) [13], [14] and lossy DC power flow [15], to solve the power flow problem in the *lossless* and *decoupled* contexts, respectively. While typical transmission lines have small losses, their presence can fundamentally change the physical behavior of the system and the solvability of the power flow problem [7], [16], and as such the algorithm proposed in [13], [14] cannot be applied. Similarly, to accurately solve the full power flow problem, the coupling between active and reactive power cannot be ignored. Our goal here is to extend this line of research to incorporate network losses and other physically realistic modelling aspects not present in the original works, and derive an *extended* FPPF algorithm to solve the AC power flow problem.

Contributions: The paper contains three main contributions. First, we develop a novel vectorization procedure for the AC power flow equations, which extends the vectorization developed in [13], [14] by incorporating resistive losses, phase-shifting transformers (PSTs), and a distributed slack bus (DSB) model [17]. Key to our vectorization is what we term the *asymmetrically weighted (AW) incidence matrix* of the weighted bidirected graph describing the transmission grid. The proposed algorithm is derived by exploiting a rank property of the AW incidence matrix. Second, we present preliminary theoretical results for a two-bus power system model, providing sufficient conditions for convergence of the algorithm towards the unique high-voltage power flow solution. Third and finally, we validate the algorithm via extensive numerical tests on standard power flow cases, and compare its performance to that of NR and the fast-decoupled (FDLF) method [18]. While our method is generally slower to converge than NR, it is more robust to changes in initialization in both lightly and heavily loaded networks. Due to space limitations, some proofs are omitted, but can be found in the thesis [19].

Notation: We use I_n to denote the $n \times n$ identity matrix, and use $\mathbf{1}_n, \mathbf{0}_n, \mathbf{0}_{n \times m}$ to denote the n -dimensional vector of all ones, zeros and the $n \times m$ zero matrix, respectively.¹ We use M^T, M^\dagger , and M^{-1} to denote the transpose, left/right inverse, and inverse of a matrix M , respectively. Given an $x \in \mathbb{R}^n$, $[x]$ denotes the diagonal matrix with x on its main diagonal, and $x > \mathbf{0}$ (resp. $x \geq \mathbf{0}, x < \mathbf{0}$) means that it is element-wise strictly positive (resp. nonnegative, strictly negative). In addition, $\mathbf{sin}(x) := [\sin(x_1) \ \cdots \ \sin(x_n)]^T$, with $\mathbf{cos}(x)$, $\mathbf{arcsin}(x)$ and \sqrt{x} defined element-wise similarly. Given $u \in \mathbb{R}^n$ and $v \in \mathbb{R}^m$, $\mathbf{col}(u, v) := [u_1, \dots, u_n, v_1, \dots, v_m]^T \in \mathbb{R}^{n+m}$.

The authors are with the Department of Electrical and Computer Engineering, University of Toronto, Toronto, ON, M5S 1A1 Canada. Email: liangjie.chen@mail.utoronto.ca, jwsimpson@ece.utoronto.ca.

¹The subscripts are omitted when the the dimensions are easy to infer from the context.

II. MODEL FORMULATION

A. Bidirected Graph Model of Transmission System

To define the bidirected graph model used in this paper, we first review the standard notion of a weakly connected directed graph (digraph) and its properties [20]. A digraph is a pair $\mathcal{G} = (\mathcal{N}, \mathcal{E})$, with the node set $\mathcal{N} := \{1, \dots, n+m\}$, and the edge set $\mathcal{E} = \{e_1, \dots, e_{|\mathcal{E}|}\} \subseteq \mathcal{N} \times \mathcal{N}$. The edge $e_k := (i, j)$ models the connection between nodes i and j , where one can travel from i to j (denoted by $i \rightarrow j$) but not vice versa. There is a weight function $W : \mathcal{E} \rightarrow (0, \infty)$ that equips each edge e_k with a positive weight w_k [21]. A digraph is simple if there are no self loops, and it is weakly connected if there exists an *undirected* path from any node to any other node in the graph. The *incidence matrix* $A \in \mathbb{R}^{(n+m) \times |\mathcal{E}|}$ of \mathcal{G} is defined element-wise as $A_{ik} = 1$ if $(i, j) \in \mathcal{E}$, and $A_{ik} = -1$ if $(j, i) \in \mathcal{E}$; otherwise, $A_{ik} = 0$. Extracting only the 1 and -1 entries, we can write $A = A^+ - A^-$, where $A_{ik}^+ = 1$ if and only if $A_{ik} = 1$, and $A_{ik}^- = 1$ if and only if $A_{ik} = -1$ [13], and allows us to define the *undirected incidence matrix* $|A|$ as $|A| := A^+ + A^-$. A *cycle matrix* $C \in \mathbb{R}^{|\mathcal{E}| \times n_c}$ has full column rank and satisfies $AC = 0$, where $n_c = |\mathcal{E}| - (n+m-1)$ [22].

In a transmission systems without PSTs, the physical branch models are symmetric with respect to changes in the current direction, resulting in a symmetric admittance matrix Y [23], and it suffices to model the circuit as a weighted digraph where each edge has one complex weight [24]. However, PSTs create asymmetries in Y , and we require a slightly more complex bidirectional digraph structure which assign different edge weights to each direction. A *bidirected graph* is a digraph $\mathcal{G}_b = (\mathcal{N}, \mathcal{E}_b)$ such that $(i, j) \in \mathcal{E}_b$ if and only if $(j, i) \in \mathcal{E}_b$ [16]. In transmission systems, a branch is a singular physical object (transmission line and/or transformer), so we use the symbol e_k to denote both directions of a branch, i.e., $\{(i, j), (j, i)\}$ rather than just (i, j) like in a digraph.² Exactly one of the two elements $\{(i, j), (j, i)\}$ is termed the “forward” edge and the other is the “backward” edge, and we may partition \mathcal{E}_b to be two disjoint sets $\mathcal{E}_b^+, \mathcal{E}_b^-$ representing the set of forward and backward edges. Similar to the weight function of a digraph \mathcal{G} , there are the “forward” and “backward” weight functions W^+, W^- mapping $\mathcal{E}_b^+, \mathcal{E}_b^-$ to $(0, \infty)$, respectively. For a branch e_k , we denote the k -th “forward” edge weight by $w_k^+ = W^+(i, j)$, and the k -th “backward” edge weight by $w_k^- = W^-(j, i)$; these weights can be collected into vectors $w^+, w^- > 0$ respectively. With this definition, every bidirected graph \mathcal{G}_b induces a digraph \mathcal{G} , whose edge set is \mathcal{E}_b^+ and weight function is W^+ . We say \mathcal{G}_b is simple and weakly connected if \mathcal{G} is simple and weakly connected. Throughout, we let A and C denote the incidence and cycle matrices of this induced forward-edge-only digraph \mathcal{G} [25].

A novel graph matrix that describes the structure of \mathcal{G}_b while accounting for the forward and backward edge weights

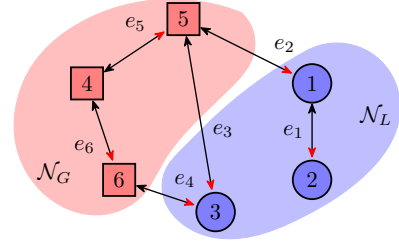


Fig. 1. Bidirected graph model of a transmission system; forward and backward directions are marked in red and black, respectively.

w^+, w^- is the *asymmetrically-weighted (AW) incidence matrix* denoted by Γ , which is defined element-wise as

$$\Gamma_{ik} := \begin{cases} w_k^+ & \text{if } (i, j) \in \mathcal{E}_b^+ \\ -w_k^- & \text{if } (i, j) \in \mathcal{E}_b^- \\ 0 & \text{otherwise.} \end{cases} \quad (1)$$

One can quickly establish that $\Gamma = A^+[w^+] - A^-[w^-]$. Similar to the construction of undirected incidence matrix $|A|$, the *undirected AW incidence matrix* is $|\Gamma| = A^+[w^+] + A^-[w^-]$. The following lemma forms a key step in the proof of Lemma 2 in Section III-B.

Lemma 1. *Suppose that \mathcal{G}_b is simple and weakly connected. Given $w^+, w^- > 0$, if there exists a nonzero $x \in \mathbb{R}^n$ such that $\Gamma^T x = 0_m$, then either $x > 0$ or $x < 0$.*

Proof. See [19, Lemma 2.1] for the proof. \square

B. Transmission System Power Flow Modelling

We model a balanced transmission network at steady state as a simple, weakly connected bidirected graph discussed previously. The node set \mathcal{N} models the buses, where $\mathcal{N}_L = \{1, \dots, n\}$ is the set of load (PQ) buses, $\mathcal{N}_G = \{n+1, \dots, n+m\}$ is the set of generator (PV) buses and $\mathcal{N} = \mathcal{N}_L \cup \mathcal{N}_G$. The edge set \mathcal{E}_b models the branches. Figure 1 demonstrates an example. Each bus $i \in \mathcal{N}$ is associated with four physical quantities of interest: voltage magnitude V_i , phase angle θ_i , real power injection P_i , and reactive power injection Q_i . For load buses, P_i, Q_i are known and V_i, θ_i are unknown. For generator buses, P_i, V_i are known and Q_i, θ_i are unknown. We can vectorize the quantities associated with each bus and partition the vectors according to the $\mathcal{N}_L, \mathcal{N}_G$ subsets as $P = \text{col}(P_L, P_G)$, $Q = \text{col}(Q_L, Q_G)$, and $V = \text{col}(V_L, V_G)$, where P, Q_L, V_G are known, and Q_G, V_L and θ are unknown. In particular, the goal of the power flow study is to solve for voltage magnitudes V_L and phases θ .³

Each branch is modelled with a PST (located at the side of bus i if $(i, j) \in \mathcal{E}_b^+$) connected to a Π -model transmission line [23, Figure 3.1]. The transmission line has a series admittance $y = g - jb$, where $g \leq 0$ is the conductance and $b > 0$ is the susceptance, and a shunt susceptance b_c . The transformer has a complex turns ratio $\tau = t \exp(j\theta_s)$ where t, θ_s respectively represent the tap ratio and phase shift. The conductance and susceptance matrices are denoted by G and B , respectively, such that $Y = G + jB$. When there is at

²In order to not double-count, we still use $|\mathcal{E}|$ to denote the number of branches in the system.

³In this study we do not consider generator reactive power limits; see [1, Example 6.11] for further information on this case.

least one PST in the system, i.e., a transformer with nonzero θ_s , both G and B become asymmetric. We partition the B matrix based on the $\mathcal{N}_L, \mathcal{N}_G$ subsets as

$$B = \left[\begin{array}{c|c} B_{LL} & B_{LG} \\ \hline B_{GL} & B_{GG} \end{array} \right].$$

Assumption 1. The sub-matrix B_{LL} is strictly diagonally dominant. If bus i is connected to bus j , then $B_{ij} > 0$.

Strict diagonal dominance implies that B_{LL} is invertible [26, Theorem 6.1.10], and physically means that capacitive shunt elements do not overcompensate the inductive network [13, Assumption 2.2]. The off-diagonal elements that correspond to network branches being positive requires that as the angle θ_s of the PST increases, the corresponding branch R/X ratio must be sufficiently small such that $b/g > \tan \theta_s$ [19, Assumption 2.2]. Together, Assumption 1 also implies that $-B_{LL}^{-1}$ is a nonnegative matrix [27, Theorem 2.3 N₃₈].

III. THE EXTENDED FIXED-POINT POWER FLOW ALGORITHM

A. A Novel Vectorization of the Power Flow Equations

Our development begins from the standard power flow equations [1] with the DSB model [17]:

$$P_i = V_i \sum_{j=1}^{n+m} V_j (G_{ij} \cos \varphi_{ij} + B_{ij} \sin \varphi_{ij}), \quad i \in \mathcal{N} \quad (2a)$$

$$Q_i = V_i \sum_{j=1}^{n+m} V_j (G_{ij} \sin \varphi_{ij} - B_{ij} \cos \varphi_{ij}), \quad i \in \mathcal{N}_L \quad (2b)$$

where φ_{ij} is the branch-wise phase difference $\theta_i - \theta_j$. In a DSB model, the nodal real power injection $P_i = \bar{P}_i + \alpha_i P_s$ is the sum of the *known* injection \bar{P}_i and a portion of the *unknown* slack power P_s . The known constants α_i are called *participation factors*, such that $\alpha_i > 0$ for all the generator buses in the distributed slack bus subset of \mathcal{N}_G and 0 otherwise, subject to $\sum_i \alpha_i = 1$.

The goal of this subsection is to vectorize (2), which will involve a change of variables. We first define the *open-circuit load voltage* $V_L^\circ \in \mathbb{R}^n$ as $V_L^\circ = -B_{LL}^{-1} B_{LG} V_G$, which is fixed since B_{LL}, B_{LG} and V_G are known, and one can show that $V_L^\circ > \mathbb{0}$ [13]. Using this quantity and the generator voltage magnitudes V_G , we let $V^\circ := \text{col}(V_L^\circ, V_G)$, and define the *normalized* load voltage as

$$v := [V_L^\circ]^{-1} V_L \in \mathbb{R}^n, \quad (3)$$

and extend this normalization scheme for all bus voltage magnitudes V_i 's as $g(v) \in \mathbb{R}^{n+m}$, where

$$g(v) := [V^\circ]^{-1} V = \begin{bmatrix} v \\ \mathbb{1}_m \end{bmatrix} \iff V = [V^\circ] g(v). \quad (4)$$

Definition 1 (Branch stiffness matrices). Given V° and the matrices G and B , the *branch stiffness matrices* are the following diagonal matrices

$$\begin{aligned} D_G^+ &= [V_i^\circ V_j^\circ G_{ij}]_{(i,j) \in \mathcal{E}_b^+} & D_G^- &= [V_i^\circ V_j^\circ G_{ji}]_{(i,j) \in \mathcal{E}_b^-} \\ D_B^+ &= [V_i^\circ V_j^\circ B_{ij}]_{(i,j) \in \mathcal{E}_b^+} & D_B^- &= [V_i^\circ V_j^\circ B_{ji}]_{(i,j) \in \mathcal{E}_b^-}. \end{aligned}$$

These matrices are extensions of those defined in [13]; the diagonal elements form the forward and backward edge weights in our bidirected graph model of the transmission system. Consequently, following Section II-A, we define the following asymmetrically weighted incidence matrices as

$$\begin{aligned} \Gamma_B &:= A^+ D_B^+ - A^- D_B^- & |\Gamma_B| &:= A^+ D_B^+ + A^- D_B^- \\ \Gamma_G &:= A^+ D_G^+ - A^- D_G^- & |\Gamma_G| &:= A^+ D_G^+ + A^- D_G^- \end{aligned} \quad (5)$$

Lastly, we define the following nonlinear map [13]

$$h(v) = \left[(A^+)^T g(v) \right] (A^-)^T g(v), \quad (6)$$

which transforms the nodal normalized voltage magnitudes $g(v)$ to branch-wise normalized voltage magnitude *products* $h(v)$. One can easily verify that the diagonal elements of $D_B^+[h(v)], D_B^-[h(v)]$ are the $V_i V_j B_{ij}, V_i V_j B_{ji}$ terms in (2), respectively, and similarly for $D_G^+[h(v)], D_G^-[h(v)]$. These elements are associated with the *branches*, and multiplication by matrices in (5) maps them into the *nodal* quantities captured by the summation in (2).

We are now ready to vectorize the power flow equations (2). We begin with the active power flow equation (2a), and expand its right-hand side to be

$$V_i^2 G_{ii} + \sum_{j \neq i} V_i V_j G_{ij} \cos \varphi_{ij} + \sum_{j \neq i} V_i V_j B_{ij} \sin \varphi_{ij}. \quad (7)$$

For the first term in (7), we extract the diagonal entries of G into the diagonal matrix $[G_{ii}]$. Applying (4), we vectorize the $V_i^2 G_{ii}$ terms for each bus by collecting them into the vector $[V^\circ][g(v)][G_{ii}][V^\circ]g(v)$. Using the incidence matrix A , we vectorize the phase differences φ_{ij} in (7) as $A^T \theta$, and we define the following change of variable

$$\psi := \sin(A^T \theta) \implies \cos(A^T \theta) = \sqrt{\mathbb{1}_{|\mathcal{E}|} - [\psi] \psi}. \quad (8)$$

Applying the asymmetrically weighted incidence matrices in (5), we can verify that

$$\begin{aligned} P &= [V^\circ][g(v)][G_{ii}][V^\circ]g(v) + |\Gamma_G|[h(v)]\sqrt{\mathbb{1}_{|\mathcal{E}|} - [\psi] \psi} \\ &\quad + \Gamma_B[h(v)]\psi \end{aligned}$$

is the vectorization of (2a) by expanding right-hand side. As mentioned at the beginning of this section, we can write the nodal power injection as $P = \bar{P} + P_s \alpha$. In power flow computations with a single slack bus, we solve for $n + m - 1$ phase angles and n load voltage magnitudes using $2n + m - 1$ power flow equations since the slack bus with fixed voltage is chosen to compensate for the unknown P_s and its corresponding active power flow equation is removed. With the DSB model, a slightly more nuanced procedure is required to eliminate this degree of freedom. To this end, since $\sum \alpha_i = 1$, we can construct a full column rank matrix $R \in \mathbb{R}^{(n+m) \times (n+m-1)}$ such that $R^T \alpha = \mathbb{0}$. Left-multiplying (9) by R^T , we eliminate P_s and obtain

$$\begin{aligned} R^T \bar{P} &= R^T \left([V^\circ][g(v)][G_{ii}][V^\circ]g(v) \right. \\ &\quad \left. + |\Gamma_G|[h(v)]\sqrt{\mathbb{1}_{|\mathcal{E}|} - [\psi] \psi} + \Gamma_B[h(v)]\psi \right), \quad (9) \end{aligned}$$

which is now a system of $n + m - 1$ active power flow equations. This reduction is a generalization of the standard single-slack-bus elimination procedure for power flow studies [19, Chapter 3.1]. Once ψ and v are known, P_s can be uniquely recovered. Denoting the right-hand side of (2a) by $\mathcal{P}(\psi, v)$, since $\sum_i \alpha_i = \mathbb{1}^\top \alpha = 1$, from (2a) we have

$$P_s \alpha = \bar{P} - \mathcal{P}(\psi, v) \implies P_s = \mathbb{1}^\top (\bar{P} - \mathcal{P}(\psi, v)).$$

We now proceed to vectorize the n reactive power flow equations (2b) corresponding to $Q_L \in \mathbb{R}^n$, the known load reactive power injections. We extract the $n \times n$ submatrix of $[B_{ii}]$, and the top $n \times |\mathcal{E}|$ submatrices of $\Gamma_G, |\Gamma_B|$, and denote them with the additional \cdot_L subscript. We may then write the vectorized reactive power flow equation as

$$Q_L = - [V_L^\circ][v][B_{ii}]_L [V_L^\circ]v + \Gamma_{G_L}[h(v)]\psi - |\Gamma_{B_L}||[h(v)]\sqrt{\mathbb{1}_{|\mathcal{E}|} - [\psi]\psi}. \quad (10)$$

Finally, we define the invertible $n \times n$ nodal stiffness matrix

$$S := \frac{1}{4}[V_L^\circ]B_{LL}[V_L^\circ],$$

and by [13, Lemma A.3], the vectorized reactive power flow equation (10) is equivalent to

$$Q_L = 4[v]S(\mathbb{1}_n - v) + \Gamma_{G_L}[h(v)]\psi + |\Gamma_{B_L}||[h(v)]\left(\mathbb{1}_{|\mathcal{E}|} - \sqrt{\mathbb{1}_{|\mathcal{E}|} - [\psi]\psi}\right). \quad (11)$$

B. Fixed-Point Reformulation of Power Flow Equations

To derive the proposed algorithm, we will manipulate the vectorized power flow equations (9), (11) into a fixed-point form. We begin with (9), and define

$$M_B = R^\top \Gamma_B \in \mathbb{R}^{(n+m-1) \times |\mathcal{E}|},$$

which can be interpreted as a ‘‘reduced’’ version of the AW incidence matrix Γ_B . The following lemma is a key result used to show the equivalence between the fixed-point reformulation and the standard power flow equations (2).

Lemma 2. *The matrix M_B has full row rank.*

Proof. We equivalently prove that M_B^\top has a trivial kernel. By contradiction, assume that there exists a nonzero $x \in \ker M_B^\top$. Then either

- 1) $x \in \ker R$, or
- 2) there exists some $y = Rx$ such that $y \in \ker \Gamma_B^\top$.

By construction, R has full column rank, so case 1) cannot occur. For case 2), suppose that such y exists and is nonzero. Denote the k -th column of Γ_B by r_k , then $\Gamma_B^\top y = \mathbb{0}$ if and only if $\langle r_k, y \rangle = 0$ for all $k = 1, \dots, |\mathcal{E}|$. By the construction of the branch stiffness matrices D_B^+, D_B^- and Assumption 1, for each $k \in \{1, \dots, |\mathcal{E}|\}$, r_k contains exactly two nonzero elements at $w_{k,i} = V_i^\circ V_j^\circ B_{ij}$ and $w_{k,j} = -V_i^\circ V_j^\circ B_{ji}$, so $\Gamma_B^\top y = \mathbb{0}$ if and only if $\langle r_k, y \rangle = V_i^\circ V_j^\circ (B_{ij}y_i - B_{ji}y_j) = 0$ for all $k = 1, \dots, |\mathcal{E}|$. However, since $V_i^\circ, V_j^\circ > 0$ and $B_{ij}, B_{ji} > 0$, y_i, y_j must be both positive, both negative, or both zero. Lemma 1 implies that $y > \mathbb{0}$ or $y < \mathbb{0}$, so $\alpha_i \geq 0$ implies that $y^\top \alpha \neq 0$ always holds. Finally, by the

construction of R , $y^\top \alpha \neq 0$ implies that $y \notin \text{im } R$, i.e., there does not exist a nonzero x such that $y = Rx \in \ker \Gamma_B^\top$ and case 2) cannot hold, which completes the proof. \square

Let K be a matrix whose columns form a basis of $\ker M_B$, so $M_B K = \mathbb{0}$. By the rank-nullity theorem and Lemma 2, K must have n_c linearly independent columns. In addition, Lemma 2 implies that matrix M_B has a right inverse denoted by M_B^\dagger , where $M_B M_B^\dagger = I_{n+m-1}$. Finally, notice that (9) is linear in $\psi \in \mathbb{R}^{|\mathcal{E}|}$ in the last term if we know v and the square root term. Since $v > \mathbb{0}$, $[h(v)]^{-1}$ exists, so we can rearrange (9) to obtain

$$\begin{aligned} \psi &= f_P(\psi, v, x_c) \\ &:= [h(v)]^{-1} M_B^\dagger R^\top (\bar{P} - [V^\circ][g(v)][G_{ii}][V^\circ]g(v) \\ &\quad - |\Gamma_G|[h(v)]\sqrt{\mathbb{1}_{|\mathcal{E}|} - [\psi]\psi}) + [h(v)]^{-1} K x_c, \end{aligned} \quad (12)$$

where the term $[h(v)]^{-1} K x_c$ characterizes the homogeneous part of the solution for ψ with an additional variable $x_c \in \mathbb{R}^{n_c}$. While (12) results in the voltage phase solution in terms of ψ , we ultimately want the bus voltage phase $\theta \in \mathbb{R}^{n+m}$. To recover θ from ψ , note that for any $k \in \mathbb{Z}$, $\sin(A^\top \theta + 2\pi k) = \psi$ and $C^\top k$ has integer elements [13]. Recalling the property that $AC = \mathbb{0}$, we must have $C^\top \arcsin(\psi) = C^\top (A^\top \theta + 2\pi k) = 2\pi C^\top k$, which results in the ‘‘loop-flow’’ constraint

$$C^\top \arcsin(\psi) \bmod 2\pi = \mathbb{0}_{n_c}. \quad (13)$$

Next, we manipulate the reactive power flow equation (11) into a fixed-point form by left-multiplying both sides of the equation by $\frac{1}{4}S^{-1}[v]^{-1}$ to obtain

$$\begin{aligned} v &= f_Q(\psi, v) := \mathbb{1}_n - \frac{1}{4}S^{-1}[v]^{-1} \left((Q_L - \Gamma_{G_L}[h(v)]\psi) \right. \\ &\quad \left. - |\Gamma_{B_L}||[h(v)]\left(\mathbb{1}_{|\mathcal{E}|} - \sqrt{\mathbb{1}_{|\mathcal{E}|} - [\psi]\psi}\right) \right). \end{aligned} \quad (14)$$

We summarize our above development in the following theorem, which is the main theoretical result of this paper.

Theorem 1 (FPPF). *Consider the normalized load voltage magnitudes $v \in \mathbb{R}^n$ defined in (3), a vector $x_c \in \mathbb{R}^{n_c}$ and the change of variable $\psi := \sin(A^\top \theta)$ defined in (8). The following statements are equivalent:*

- (i) (θ, V_L) solves the vectorized power flow equations (9), (11);
- (ii) (ψ, v, x_c) satisfy the fixed point equations (12), (14), and the loop flow constraint (13).

When there are no network losses and PSTs in the system, Theorem 1 recovers [13, Theorem 3.5]. If the system is radial, i.e., $|\mathcal{E}| = n + m - 1$, then the loop flow constraint (13) and the homogeneous solution in (12) are not required since the kernel of the incidence matrix A is trivial [20], so $n_c = 0$ and we no longer need the variable x_c .

C. The Extended FPPF Algorithm

Based on Theorem 1, we propose the following extended fixed-point power flow algorithm, which will be tested extensively in Section V.

Algorithm 1 The extended fixed-point power flow algorithm

Require: Power flow data, tolerance ϵ , max. iterations L
 $v^k \leftarrow V_L/V_L^\circ$, $\psi^k \leftarrow \mathbf{sin}(A^\top\theta)$, $x_c^k \leftarrow \mathbb{0}_{n_c}$
 $k \leftarrow 0$
 Compute power balance mismatch with ψ^k, v^k
while mismatch $> \epsilon$ and $k < L$ **do**
 $v^{k+1} \leftarrow f_Q(\psi^k, v^k, x_c^k)$
if $n_c > 0$ **then**
 $x_c^{k+1} \leftarrow \text{Newton step on } C^\top \mathbf{arcsin}(\psi^k) = \mathbb{0}_{n_c}$
 $\psi^{k+1} \leftarrow f_P(\psi^k, v^{k+1}, x_c^{k+1})$
 Compute power balance mismatch with ψ^{k+1}, v^{k+1}
 $k \leftarrow k + 1$
return ψ^{k+1}, v^{k+1} , power balance mismatch

The power flow data consist of the matrices and vectors related to the network topology, admittance matrix, loading profiles and other constants used in the reformulation; see [19, Section 6.1] for the discussion on their construction. The Newton step to evaluate x_c^{k+1} is

$$x_c^{k+1} = x_c^k - (J_c^k)^{-1} C^\top \mathbf{arcsin}(\psi^k),$$

where $J_c^k := C^\top (|I_{\mathcal{E}}| - [\psi^k]^2)^{-1/2} [h(v^{k+1})]^{-1} K$ is the Jacobian matrix of the constraint evaluated at ψ^k ; note that J_c^k is computed using the most up-to-date v^{k+1} .

Remark 1 (Update order). In the spirit of [28], we use the most updated version of a variable to evaluate the update of the other variables. For the numerical simulations in Section V, we follow a “ v - x_c - ψ ” order: we first compute v^{k+1} with ψ^k, v^k, x_c^k , then compute x_c^{k+1} with v^{k+1} instead of v^k , and finally ψ^{k+1} with both v^{k+1} and x_c^{k+1} . Other orders are also possible; see [19, Section 6.2.1] for a detailed discussion on the effect of different update orders. \square

IV. ANALYSIS OF ALGORITHM FOR TWO-BUS SYSTEM

As preliminary theoretical analysis of our approach, we conduct a convergence analysis of the FPPF algorithm on the two-bus power flow problem [29]. Since a fixed-point algorithm like ours naturally leads to a contraction analysis, we re-frame the problem as one of constructing a compact invariant set on which the FPPF algorithm is a contraction.

A. Problem Setup

Consider the two-bus model in Figure 2, where bus 2 is the only PV/slack bus, bus 1 is the PQ bus, and the branch parameters t, θ_s, g, b, b_c are as described in Section II-B.

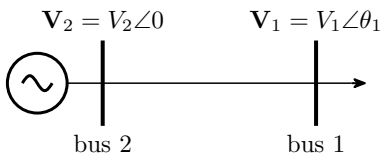


Fig. 2. Two bus system

Let $\bar{t} := t - 1$, we define the following system constants

$$\tilde{g} := \frac{g \cos \theta_s - b \sin \theta_s}{\bar{t} + 1}, \quad \tilde{b} := \frac{b \cos \theta_s + g \sin \theta_s}{\bar{t} + 1}, \quad \hat{b} := b - \frac{b_c}{2}.$$

Next, let $\rho := g/\hat{b}$, $\tilde{\rho} := \tilde{g}/\tilde{b}$ be two constants that quantify the system R/X ratio; realistically, $\rho \geq 0$, and Assumption 1 implies $\tilde{\rho} \geq 0$. We define real and reactive power loading margins as

$$\tilde{\gamma}_P := \frac{\bar{P}_1}{\tilde{b} V_1^\circ V_2^\circ}, \quad \tilde{\gamma}_Q := \frac{Q_1}{\tilde{b} V_1^\circ V_2^\circ},$$

where the open-circuit load voltage evaluates to be $V_1^\circ = (\tilde{b}/\hat{b})V_2$. Making the change of variable $x := v - 1$ and defining the state vector $\xi := (\psi, x)$, we can write the FPPF algorithm update rule as

$$\xi_{k+1} = \underbrace{\begin{bmatrix} \frac{-\tilde{\gamma}_P}{x_k + 1} + \rho(x_k + 1) - \tilde{\rho}\sqrt{1 - \psi_k^2} \\ \frac{\tilde{\gamma}_Q}{x_k + 1} - \tilde{\rho}\psi_{k+1} + \sqrt{1 - \psi_{k+1}^2} - 1 \end{bmatrix}}_{F_\mu(\xi_k)}. \quad (15)$$

The μ subscript in (15) refers to the vector of “perturbations”

$$\mu := [g \quad b_c \quad \bar{t} \quad \theta_s]^\top.$$

If $\mu = \mathbb{0}$, then the system is lossless, the transformer is absent, and the branch is simply a series reactance given by $1/b$; in this case, $\rho = \tilde{\rho} = 0$. We call this case the “nominal system” and denote the corresponding mapping that defines the update rule by F_0 , otherwise we call it the “full system”.

The ultimate goal of the ensuing analysis is to (i) construct a F_μ -invariant set for (15), and (ii) provide sufficient conditions that F_μ is a contraction on this set; this will guarantee convergence of (15) to a (locally) unique solution. Our approach will be to develop results for F_0 , and then extend these results to F_μ for sufficiently small μ values.

B. Nominal System Results

When $\mu = \mathbb{0}$, by construction $\hat{b} = \tilde{b} = b > 0$, $\tilde{g} = g = 0$, and $V_1^\circ = V_2^\circ$. We denote the reduced constants $\tilde{\gamma}_P, \tilde{\gamma}_Q$ by γ_P, γ_Q , respectively. The assumption below provides a crucial characterization of permissible loading margins.

Assumption 2. $0 < 4\gamma_P^2 - 4\gamma_Q < 1$.

Assumption 2 is a standing assumption for the rest of this section. It states that the load is inductive, and restricts the amount of loading in the system⁴. Now, define the compact and convex set

$$\mathcal{A}(k_1, k_2) := \{\xi : |\psi| \leq k_1, |x| \leq k_2\}, \quad (16)$$

which is a closed box in \mathbb{R}^2 centered at the origin, parameterized by some $k_1, k_2 > 0$ to be determined.

Theorem 2. Let $k_1^- := -\gamma_P/(1 - k_2^-)$, where

$$k_2^- := 1 - \sqrt{\frac{1}{2} + \gamma_Q + \sqrt{\frac{1}{4} + \gamma_Q - \gamma_P^2}},$$

$$k_2^+ := 1 - \sqrt{\frac{1}{2} + \gamma_Q - \sqrt{\frac{1}{4} + \gamma_Q - \gamma_P^2}}.$$

⁴It is physically valid for γ_P, γ_Q to be both zero, but we are interested in the case of a strictly positive active power injection at the generator bus.

The set $\mathcal{A}(k_1, k_2)$ is F_0 -invariant for any $k_1 \in [k_1^-, 1]$ and $k_2 \in [k_2^-, k_2^+]$.

Proof. See [19, Section 5.2.1] for the proof. \square

We are especially interested in the *smallest* F_0 -invariant set denoted by $\mathcal{A}^- := \mathcal{A}(k_1^-, k_2^-)$. In fact, one can verify by direct substitution that $\xi = [k_1^- - k_2^-]^\top$ is the desired high-voltage solution, and it exists on the boundary of \mathcal{A}^- .

Theorem 3. F_0 is a contraction on \mathcal{A}^- in the ℓ_∞ norm.

Proof. See [19, Section 5.2.2] for the proof. \square

The above results implicitly recover the calculations in [29, Chapter 2], along with the existence/uniqueness result of [14] when restricted to the two-bus case.

C. Full System Analysis

We now return to the update rule (15) for $\mu \neq 0$. First, note that we can write $\tilde{\gamma}_P = k_\mu \gamma_P$ and $\tilde{\gamma}_Q = k_\mu \gamma_Q$, where $k_\mu := (b\hat{b})/\tilde{b}^2$. Let $\epsilon_1 = \epsilon_1(\mu, \gamma_P, \gamma_Q)$ and $\epsilon_2 = \epsilon_2(\mu, \gamma_P, \gamma_Q)$ be nonnegative constants to be determined, and define the set

$$\mathcal{A}_\epsilon(k_1, k_2) := \mathcal{A}(k_1 + \epsilon_1, k_2 + \epsilon_2),$$

then we can define $\mathcal{A}_\epsilon^- := \mathcal{A}_\epsilon(k_1^- + \epsilon_1, k_2^- + \epsilon_2)$. Intuitively, this set is “slightly expanded” from \mathcal{A}^- when $\mu \neq 0$. We now derive a condition on $\epsilon := (\epsilon_1, \epsilon_2)$ such that \mathcal{A}_ϵ^- is F_μ -invariant, which is true if and only if for every $\xi_k \in \mathcal{A}_\epsilon^-$,

$$|\psi_{k+1}| = \left| \frac{-k_\mu \gamma_P}{x_k + 1} + \rho(x_k + 1) - \tilde{\rho} \sqrt{1 - \psi_k^2} \right| \leq k_1^- + \epsilon_1,$$

$$|x_{k+1}| = \left| \frac{k_\mu \gamma_Q}{x_k + 1} - \tilde{\rho} \psi_{k+1} + \sqrt{1 - \psi_{k+1}^2} - 1 \right| \leq k_2^- + \epsilon_2.$$

By triangle inequality and the fact that $|x_k| \leq k_2^-$, the $|\psi_{k+1}|$ term in first inequality can be upper bounded by

$$\frac{-k_\mu \gamma_P}{1 - k_2^- - \epsilon_2} + \rho(1 + k_2^- + \epsilon_2) + \tilde{\rho}.$$

Adding and subtracting a $k_1^- = \gamma_P/(1 - k_2^-)$ in the expression above, if ϵ satisfies

$$\frac{-k_\mu \gamma_P}{1 - k_2^- - \epsilon_2} + \frac{\gamma_P}{1 - k_2^-} + \rho(1 + k_2^- + \epsilon_2) + \tilde{\rho} \leq \epsilon_1, \quad (17a)$$

then any $|\psi_k| \leq k_1^- + \epsilon_1$ implies $|\psi_{k+1}| \leq k_1^- + \epsilon_1$. Note that we also need $\epsilon_2 < 1 - k_2^-$ to prevent division by zero in (17a). Similarly, the $|x_{k+1}|$ term in the second inequality can be upper bounded by

$$\frac{-k_\mu \gamma_Q}{1 - k_2^- - \epsilon_2} + \tilde{\rho}(k_1^- + \epsilon_1) - \sqrt{1 - (k_1^- + \epsilon_1)^2} + 1.$$

Adding and subtracting a k_2^- above, if ϵ satisfies

$$\frac{-k_\mu \gamma_Q}{1 - k_2^- - \epsilon_2} + (1 - k_2^-) + \tilde{\rho}(k_1^- + \epsilon_1) - \sqrt{1 - (k_1^- + \epsilon_1)^2} \leq \epsilon_2, \quad (17b)$$

then any $|x_k| \leq k_2^- + \epsilon_2$ implies $|x_{k+1}| \leq k_2^- + \epsilon_2$. Note that we also require $\epsilon_1 \leq 1 - k_1^-$ for the square root term to be

real-valued. Since F_μ is a composition of C^1 functions and is thus C^1 on \mathcal{A}_ϵ^- , by Brouwer’s fixed-point theorem [30, Theorem 52], the bounding steps above imply the existence of a solution in the set \mathcal{A}_ϵ^- , stated below.

Proposition 1. *If there exists an ϵ such that the inequalities in (17) hold, then the set \mathcal{A}_ϵ^- is F_μ -invariant and the two-bus system possesses a power flow solution in the set \mathcal{A}_ϵ^- .*

As the inequalities (17) do not appear to admit straightforward analytical solutions, we will proceed via continuity and argue that (17) are feasible in ϵ for sufficiently small μ . Of course, any ϵ that satisfies (17) at the boundary trivially satisfies the inequalities themselves; we proceed by focusing on (17) with equality sign. Rearranging (17) and moving all terms to one side, we define the mapping $E : \mathcal{D}_\epsilon \times \mathbb{R}^4 \rightarrow \mathbb{R}^2$, where $\mathcal{D}_\epsilon \subset [0, 1 - k_1^-] \times [0, 1 - k_2^-] \subset \mathbb{R}^2$ is an open set and $E = (E_1, E_2)$ is defined by

$$E_1(\epsilon, \mu) = \frac{-k_\mu \gamma_P}{1 - k_2^- - \epsilon_2} + \frac{\gamma_P}{1 - k_2^-} + \rho(1 + k_2^- + \epsilon_2) + \tilde{\rho} - \epsilon_1 = 0,$$

$$E_2(\epsilon, \mu) = \frac{-k_\mu \gamma_Q}{1 - k_2^- - \epsilon_2} + (1 - k_2^-) + \tilde{\rho}(k_1^- + \epsilon_1) - \sqrt{1 - (k_1^- + \epsilon_1)^2} - \epsilon_2 = 0.$$

That is, given a μ , an ϵ that satisfies $E(\epsilon, \mu) = 0$ satisfies (17) with equality sign. Using straightforward algebra and writing k_1^-, k_2^- in terms of the loading margins γ_P, γ_Q , we can verify that when $\mu = 0$, we can simply choose $\epsilon = 0$ to satisfy $E(\epsilon, 0) = 0$ [19, Proposition 5.1]. Using this fact, we can certify that a general local solution to $E(\epsilon, \mu) = 0$ exists when $\mu \neq 0$, as summarized below.

Proposition 2. *There exists a nonempty open subset, $\mathcal{U} = \mathcal{U}_\epsilon \times \mathcal{U}_\mu \subset \mathcal{D}_\epsilon \times \mathbb{R}^4$ and a unique C^1 function $f : \mathcal{U}_\mu \rightarrow \mathbb{R}^2$, such that $(0_2, 0_4) \in \mathcal{U}$, $f(0_4) = 0_2$ and $E(f(\mu), \mu) = 0_2$ for all $\mu \in \mathcal{U}_\mu$. That is, for each sufficiently small μ , there exists a unique $\epsilon = f(\mu)$ satisfying (17) with equality sign; consequently, the set \mathcal{A}_ϵ^- contains a power flow solution of the two-bus system.*

The proof relies on the implicit function theorem [31], which we can apply since E is a composition of C^1 functions and is thus C^1 . The existence of a solution then follows from Proposition 1. The detailed calculations can be found in [19, Section 5.3.1].

Similar to the result in Theorem 3, the proposition below states that F_μ is further a contraction on \mathcal{A}_ϵ^- , so the FPPF algorithm (15) will converge linearly to the unique solution from any initial condition in \mathcal{A}_ϵ^- .

Proposition 3. *For each sufficiently small μ , there exists ϵ such that \mathcal{A}_ϵ^- is F_μ -invariant and F_μ is a contraction on \mathcal{A}_ϵ^- in the ℓ_∞ norm.*

The proof relies on the fact that F_μ is a C^1 function, so we can compute the ℓ_∞ norm of its Jacobian matrix evaluated at any $\xi_k \in \mathcal{A}_\epsilon^-$. Thus, by Theorem 3, we can argue by continuity that a sufficiently small μ implies that F_μ is a

TABLE I
ITERATIONS REQUIRED TO CONVERGE

Test case	Base loading			High loading		
	NR	FDLF	FPPF	NR	FDLF	FPPF
9 bus system	4	6	8	5	29	22
30 bus system	3	11	18	6	28	22
PEGASE 89	4	9	10	6	26	23
118 bus system	4	11	11	6	33	25
300 bus system	5	15	33	6	33	33
PEGASE 1354	5	11	42	5	25	42
PEGASE 2869	5	11	42	6	29	42
PEGASE 9241	6	17	46	6	23	47

contraction on \mathcal{A}_ϵ^- in the ℓ_∞ norm. See [19, Section 5.3.2] for the detailed derivations. In sum, the above results show that the extended FPPF inherits the convergence properties of the original lossless FPPF [13], at least for sufficiently small losses and transformer tap ratios. Improvement and extension of this analysis to multi-bus systems is a topic of ongoing work.

V. NUMERICAL TESTS

We now illustrate the effectiveness of Algorithm 1 using a selection of MATPOWER test cases, and compare its behaviour to that of the conventional NR and FDLF methods. Due to space limitations we focus on only two aspects of algorithm performance: (i) iterations required for convergence, and (ii) sensitivity to the initial bus voltage values. For convergence criteria, we set the maximum iteration count to be 100, and the power balance mismatch tolerance to be 10^{-8} p.u. for all three algorithms. We use the default single-slack bus model in these test cases since NR and FDLF are not implemented to accommodate the DSB model in [32].

Remark 2 (R/X Ratios). During testing, it was observed that Algorithm 1 can fail in test cases with unrealistically high branch R/X ratios, which do indeed occur for a small number of branches in certain MATPOWER test cases. The FDLF and — to a lesser extent — NR algorithms also struggle in cases with high R/X ratios. As practical transmission networks typically have low branch R/X ratios⁵, in the tests that follow we cap all branch R/X ratios at 0.8, which involves modifying less than 1% of the branches in each case considered. This modification ensures that the considered cases are convergent for all algorithms. \square

A. Iterations Required for Convergence

Here, we compare the number of iterations each algorithm required to converge using the “flat-start” initial condition ($V_L = \mathbf{1}_n$ and $\theta = \mathbf{0}_n$). We present the simulation results based on two loading scenarios: (i) base loading, which is the default values on the test systems, and (ii) high loading, which is computed by continuation power flow (CPF). For the latter scenario, the base power generation and demand are set to be 90% of the way to the power flow insolvability boundary, yielding highly stressed test systems.

⁵The mean R/X ratios for the systems in Table I are approximately 0.11, 0.37, 0.14, 0.25, 0.19, 0.15, 0.15, and 0.19.

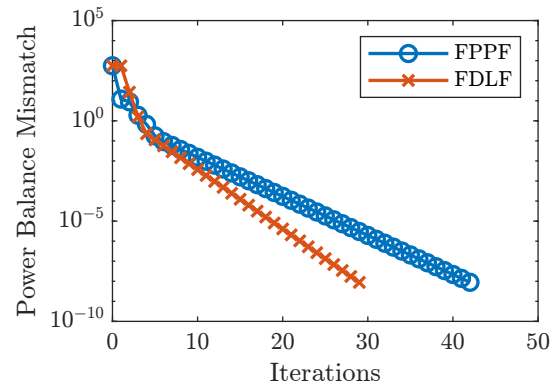


Fig. 3. Mismatch trajectories of FPPF and FDLF on the PEGASE 2869 system with high loading.

TABLE II
ALGORITHM SUCCESS RATE (%), 118 BUS SYSTEM

δ	Base loading			High loading		
	NR	FDLF	FPPF	NR	FDLF	FPPF
0.1	100.0	100.0	100.0	100.0	100.0	100.0
0.2	98.8	100.0	100.0	98.8	100.0	100.0
0.3	65.6	100.0	100.0	66.7	100.0	100.0
0.4	6.9	100.0	100.0	7.7	100.0	100.0
0.5	0.0	100.0	100.0	0.0	100.0	100.0
0.9	0.0	100.0	100.0	0.0	98.7	100.0
0.95	0.0	100.0	100.0	0.0	89.0	98.9

Table I shows the number of iterations each algorithm takes to converge. When NR converges successfully, it consistently outperforms both FDLF and FPPF due to its quadratic convergence rate. The iterations required by FDLF and FPPF are comparable, though FDLF is more susceptible to changes in loading level on large systems (300 buses or more). However, both FPPF and FDLF exhibit linear convergence rates, as shown in Figure 3.

B. Sensitivity to Initialization

Next, we test each algorithm’s sensitivity to bus voltage initialization. For a constant $\delta \in (0, 1)$, we generate 1000 random samples of initial voltage magnitudes $V_{L,\text{init}}^{[k]} \in \mathbb{R}^n$, where the superscript $[k]$ represents the k -th sample. Each element of $V_{L,\text{init}}^{[k]}$ is sampled from a uniform distribution on the interval $[1 - \delta, 1 + \delta]$, and we set the initial load bus voltage magnitude $V_L^0 = V_{L,\text{init}}^{[k]}$, for $k = 1, \dots, 1000$ while keeping $\theta = \mathbf{0}_{n+m}$.

We first compute the known high voltage solution using NR with flat-start voltages, then compare this solution against the ones returned by NR, FDLF and FPPF using the random voltage initializations. If the solution returned does not match the known solution up to a small tolerance, or if the algorithm fails to converge, then the sample is marked as unsuccessful, otherwise it is successful. Table II demonstrates each algorithm’s success rate for different δ on the 118 bus system.

Evidently, NR is the least robust against the random voltage magnitude initialization since its success rate drastically decreases as δ increases. This observation matches the well-known fact that the convergence of NR is extremely sensitive

to the initial condition selection [6]. FDLF performs almost as well as FPPF until δ gets close to 1 in the high loading scenario, where a small number of samples fail to converge.

When the FPPF converges, it always converges to the known high voltage solution, and is the most robust out of all three algorithms under this random initialization scheme. This may be a valuable feature in power flow problems where there is considerable uncertainty about the location of the solution. Alternatively, the FPPF may be valuable as a warm-start tool for a NR-based solver. Curiously, when the FPPF algorithm fails, it is because during the iterations, the implicit constraint that $\|\psi\|_\infty \leq 1$ in (12) is violated; this constraint keeps ψ real-valued. A rigorous procedure to ensure that this constraint remains satisfied during iterations is a subject of ongoing work.

VI. CONCLUSION

We have derived and tested a new algorithm for the AC power flow problem by extending the lossless FPPF algorithm of [13] to accommodate network loss, phase-shifting transformers, and the distributed slack bus model. As a first step in the theoretical analysis of the algorithm, we studied it on the two-bus system and presented sufficient conditions for the algorithm to converge to the desired solution. We also tested the numerical performance of the proposed FPPF algorithm on standard small- and large-scale test cases. Avenues of future work include improving the algorithm's robustness against branches with high R/X ratios (potentially by modifying the fixed-point reformulation) and extending the convergence conditions of the proposed FPPF algorithm on the two-bus system to general systems.

REFERENCES

- [1] J. Glover, T. Overbye, and M. Sarma, *Power System Analysis and Design*, 5th ed. Cengage Learning, 2016.
- [2] D. K. Molzahn and I. A. Hiskens, "A survey of relaxations and approximations of the power flow equations," *Foundations and Trends in Electric Energy Systems*, vol. 4, no. 1-2, pp. 1–221, 2019.
- [3] D. Mehta, D. K. Molzahn, and K. Turitsyn, "Recent advances in computational methods for the power flow equations," in *Proc. ACC*, 2016, pp. 1753–1765.
- [4] J. Lindberg, A. Zachariah, N. Boston, and B. Lesieutre, "The distribution of the number of real solutions to the power flow equations," *IEEE Trans. Power Syst.*, 2022. DOI: 10.1109/TPWRS.2022.3170232.
- [5] D. Lee, H. D. Nguyen, K. Dvijotham, and K. Turitsyn, "Convex restriction of power flow feasibility sets," *IEEE Trans. Control Net. Syst.*, vol. 6, no. 3, pp. 1235–1245, 2019.
- [6] W. F. Tinney and C. E. Hart, "Power flow solution by newton's method," *IEEE Trans. Power Apparatus & Syst.*, vol. PAS-86, no. 11, pp. 1449–1460, 1967.
- [7] B. Stott, J. Jardim, and O. Alsac, "Dc power flow revisited," *IEEE Trans. Power Syst.*, vol. 24, no. 3, pp. 1290–1300, 2009.
- [8] L. Chen and J. E. Tate, *Hot-starting the ac power flow with convolutional neural networks*, 2020. arXiv: 2004.09342 [eess.SY].
- [9] B. Cui and X. A. Sun, *Solvability of power flow equations through existence and uniqueness of complex fixed point*, 2019. arXiv: 1904.08855 [cs.SY].
- [10] S. Bolognani and S. Zampieri, "On the existence and linear approximation of the power flow solution in power distribution networks," *IEEE Trans. Power Syst.*, vol. 31, no. 1, pp. 163–172, 2015.
- [11] C. Wang, A. Bernstein, J.-Y. Le Boudec, and M. Paolone, "Explicit conditions on existence and uniqueness of load-flow solutions in distribution networks," *IEEE Trans. Smart Grid*, vol. 9, no. 2, pp. 953–962, 2016.
- [12] A. Bernstein and E. Dall'Anese, "Linear power-flow models in multiphase distribution networks," in *2017 IEEE PES ISGT-Europe*, 2017, pp. 1–6.
- [13] J. W. Simpson-Porco, "A theory of solvability for lossless power flow equations – Part I: Fixed-point power flow," *IEEE Trans. Control Net. Syst.*, vol. 5, no. 3, pp. 1361–1372, 2018.
- [14] J. W. Simpson-Porco, "A theory of solvability for lossless power flow equations – Part II: Conditions for radial networks," *IEEE Trans. Control Net. Syst.*, vol. 5, no. 3, pp. 1373–1385, 2018.
- [15] J. W. Simpson-Porco, "Lossy DC power flow," *IEEE Trans. Power Syst.*, vol. 33, no. 3, pp. 2477–2485, 2018.
- [16] R. Delabays, S. Jafarpour, and F. Bullo, "Multistability and anomalies in oscillator models of lossy power grids," *Nature Communications*, vol. 13, no. 1, p. 5238, Sep. 2022.
- [17] S. Dhople, Y. Chen, A. Al-Digs, and A. Domínguez-García, "Reexamining the distributed slack bus," *IEEE Trans. Power Syst.*, vol. 35, no. 6, pp. 4870–4879, 2020.
- [18] B. Stott and O. Alsac, "Fast decoupled load flow," *IEEE Trans. Power Apparatus & Syst.*, vol. PAS-93, no. 3, pp. 859–869, 1974.
- [19] L. Chen, "A fixed-point algorithm for the AC power flow problem," M.A.Sc. Thesis, University of Toronto, 2022. [Online]. Available: <https://www.control.toronto.ca/~jwsimpson/thesis/lc-masc.pdf>.
- [20] F. Bullo, *Lectures on Network Systems*, 1.6. Kindle Direct Publishing, 2022, ISBN: 978-1986425643.
- [21] T. H. Cormen, C. E. Leiserson, R. L. Rivest, and C. Stein, *Introduction to Algorithms* (The MIT Press), 3rd ed. London, England: MIT Press, Jul. 2009.
- [22] T. Kavitha, C. Liebchen, K. Mehlhorn, *et al.*, "Cycle bases in graphs characterization, algorithms, complexity, and applications," *Computer Science Review*, vol. 3, no. 4, pp. 199–243, 2009.
- [23] R. D. Zimmerman and C. E. Murillo-Sanchez, *MATPOWER User's Manual, Version 7.1*, 2020.
- [24] F. Dörfler, J. W. Simpson-Porco, and F. Bullo, "Electrical networks and algebraic graph theory: Models, properties, and applications," *Proceedings of the IEEE*, vol. 106, no. 5, pp. 977–1005, 2018.
- [25] E. Lawler, *Combinatorial Optimization: Networks and Matroids*. Dover Publications, 2001, ISBN: 9780486414539.
- [26] R. Horn and C. Johnson, *Matrix Analysis*, 2nd ed. Cambridge University Press, 2013.
- [27] A. Berman and R. J. Plemmons, *Nonnegative Matrices in the Mathematical Sciences*. Academic Press, Dec. 1979.
- [28] F. F. Wu, "Theoretical study of the convergence of the fast decoupled load flow," *IEEE Trans. Power Apparatus & Syst.*, vol. 96, no. 1, pp. 268–275, 1977.
- [29] T. Van Cutsem and C. Vournas, *Voltage Stability of Electric Power Systems*. Boston, MA: Springer, 1998.
- [30] C. C. Pugh, *Real Mathematical Analysis*, 2nd ed. Springer Cham, 2015.
- [31] O. de Oliveira, "The implicit and the inverse function theorems: Easy proofs," *Real Anal. Exchange*, vol. 39, no. 1, p. 207, 2014.
- [32] R. Zimmerman, C. Murillo-Sánchez, and R. Thomas, "Matpower: Steady-state operations, planning, and analysis tools for power systems research and education," *IEEE Trans. Power Syst.*, vol. 26, no. 1, pp. 12–19, 2011.